A&A 516, A89 (2010)
DOI: 10.1051/0004-6361/200912579

Astronomy & Astrophysics

A non-hydrodynamical model for acceleration of line-driven winds in active galactic nuclei

G. Risaliti[1,2] and M. Elvis[2]

[1] INAF – Osservatorio Astrofisico di Arcetri, Largo E. Fermi 5, 50125 Firenze, Italy
e-mail: risaliti@arcetri.astro.it
[2] Harvard-Smithsonian Center for Astrophysics, 60 Garden Street, Cambridge, MA 02138, USA

Received 26 May 2009 / Accepted 4 November 2009

ABSTRACT

Context. Radiation driven winds are the likely origin of AGN outflows, and are believed to be a fundamental component of the inner structure of AGNs. Several hydrodynamical models have been developed, showing that these winds can be effectively launched from AGN accretion disks.
Aims. Here we want to study the acceleration phase of line-driven winds in AGNs, in order to examine the physical conditions required for the existence of such winds for a wide variety of initial conditions.
Methods. We built a simple and fast non-hydrodynamic model QWIND, where we assume that a wind is launched from the accretion disk at supersonic velocities of a few 100 km s^{-1}, and we concentrated on the subsequent supersonic phase, when the wind is accelerated to final velocities up to 10^4 km s^{-1}.
Results. We show that, with a set of initial parameters in agreement with observations in AGNs, this model can produce a wind with terminal velocities on the order of 10^4 km s^{-1}. There are three zones in the wind, only the middle one of which can launch a wind: in the inner zone the wind is too ionized and so experiences only the Compton radiation force, which is not effective in accelerating gas. This inner "failed wind" is important for shielding the next zone by lowering the ionization parameter there. In the middle zone the lower ionization of the gas leads to a much larger radiation force and the gas achieves escape velocity This middle zone is quite thin (about 100 gravitational radii). The outer, third zone is shielded from the UV radiation by the central wind zone, so does not achieve a high enough acceleration to reach escape velocity. We also describe a simple analytic approximation of our model, in which we neglect the effects of gravity during the acceleration phase. This analytic approach agrees with the results of the numerical code, and is a powerful way to check whether a radiation driven wind can be accelerated with a given set of initial parameters.
Conclusions. Our analytical analysis and the fast QWIND model agree with more complex hydrodynamical models, and allow exploration of the dependence of the wind properties for a wide set of initial parameters: black hole mass, Eddington ratio, initial density profile, X-ray to UV ratio.

Key words. galaxies: active – quasars: general – acceleration of particules

1. Introduction

Outflowing winds are now believed to be common, and quite possibly ubiquitous, in the inner parts of active galactic nuclei (AGNs) and quasars. The most striking evidence comes from the 10% of broad absorption line (BAL) quasars that show blueshifted absorption lines spanning 10–20 thousand km s^{-1}. Less spectacular, but more common, evidence of outflows comes from the 50% of AGNs with narrow absorption lines (NALs) both UV and X-ray (Reynolds 1997; George et al. 1998; Crenshaw et al. 1999; Krongold et al. 2003; Vestergaard 2003; Piconcelli et al. 2005; Ganguly & Brotherton 2007).

Several attempts have been made to explain the origin of such winds. Two main scenarios have been suggested: magnetically driven winds (Blandford & Payne 1982; Konigl & Payne 1994; Konigl & Kartje 1994; Everett & Murray 2007), or radiation driven winds. One of the most promising explanations is through radiation line-driven winds arising from the accretion disk. The physics of radiation line-driven winds, based on the work of Sobolev (1960), was developed by Castor et al. (1975, hereafter CAK), and Abbott (1982, 1986) for winds from hot stars. CAK showed that resonance line absorption in an accelerating flow could be hundreds of times more effective than pure electron scattering. More recently the same theory has been applied to accretion disks in compact binaries (Proga et al. 1998) and to AGN disks (Murray et al. 1995; Proga et al. 2000, hereafter P00, Proga 2003). These authors use the powerful hydrodynamical code ZEUS2D (Stone & Norman 1992) to solve the wind equations, assuming a Shakura-Sunyaev (1972, hereafter SS) α-disk, and plausible initial conditions. The main results of these papers are: (1) the demonstration that a wind can be launched and accelerated up to velocities on the order of 10^4 km s^{-1}; and (2) the determination of the wind geometry and physical state for the given starting conditions. These models have been tested with several different choices of the initial conditions (Proga & Kallman 2004), showing that a wind can arise for a wide range of black hole mass and accretion rates.

Other recent improvements in this field are the modeling of Schurch & Done (2007), where the interaction between the X-ray radiation and the outflowing wind is throughly analyzed, and the analysis of possible effects of radiation winds at greater distances from the accretion disk, such as on a parsec-scale X-ray heated torus (Dorodnitsyn et al. 2008), and on large-scale AGN outflows (Kurosawa & Proga 2009).

One key aspect of the physics of radiation driven winds, which emerges clearly from the models mentioned above, is that

regardless of the details of the initial launching phase, it is impossible to avoid the strong, probably dominant, effect of radiation pressure in the subsequent acceleration phase, where the wind gains more than 99% of its kinetic energy. This is easily estimated from the comparison between the amount of momentum absorbed by the gas and its final momentum. For example, Hamann (1998) estimates that at least ~25% of the UV radiation emitted by the BAL quasar PG 1254+047 is absorbed by a gas with column density of 10^{23} cm^{-2}. It is sufficient that the luminosity of this source is 10% of the Eddington luminosity to conclude that the momentum in the outflowing wind is close to what is absorbed in the UV wavelength range.

The distinction between the *launching* and *acceleration* phases of an accretion disk wind, which we made above, allows modeling of the problem to be separated into these two parts. The *launching* phase has been investigated in several numerical simulations, both in hydrodynamical (Ohsuga et al. 2005) and magneto-hydrodynamical (Hawley & Krolik 2006) regimes. Recently, the creation of outflows from accretion disks has been investigated through MHD simulations including the effects of radiation pressure (Ohsuga et al. 2009).

The main aim of the work presented here is to explore a wide set of initial conditions for the *acceleration* phase of a wind in AGN using a deliberately simplified approach in the hope that this can produce an intuitive understanding of quasar winds and so guide future detailed simulations. We make use both of analytic approximations and of a simplified numerical code for quasar winds, which we have named *QWIND*. *QWIND* treats the radiation force mechanism in detail, but not the internal gas pressure in the wind. As the wind velocity in the acceleration phase is always many times the thermal velocity of the wind gas, this is a reasonable approach.

Our study is motivated by the observations of fast outflows in BAL quasars (Weymann 1997), by photometric evidence of a highly flattened structure in BAL winds (Ogle et al. 1999) and by results suggesting an axially symmetric, but not spherical, spatial distribution of the broad emission line (BEL) gas (Wills & Browne 1986; Brotherton 1996; Maiolino et al. 2001; Rokaki et al. 2003). Elvis (2000) has proposed a specific quasar unification model based on this kind of structure. This model predicts that a geometrically thin, funnel-shaped outflow is present in all AGNs and quasars, which allows the observational properties of the different classes of sources to be explained through orientation effects. This model provided our initial motivation, as we suspected that a radiation driven wind might naturally create a thin, funnel-shaped structure.

We therefore developed the *QWIND* model in order to easily and quickly explore the acceleration of a radiation-driven wind for the huge range of physically possible initial conditions, in terms of black hole mass, accretion rate, relative strength of the X-ray radiation, and the initial density and temperature of the outflowing gas. Our approach does not add more physical insight to the individual wind solutions than the already available hydrodynamical models mentioned above, but does allow a much wider exploration of the initial parameters space in a reasonable length of time.

The purpose of this paper is to present the model code, *QWIND*, and to demonstrate that *QWIND* produces results that also agree with both an analytic treatment and with the more complex and detailed approach of P00. Some of these results are physically interesting. The structure of this paper is the following. In Sect. 2 we briefly review previous results on the topic of radiation-driven winds. In Sect. 3 we present the *QWIND* code and show examples of its possible applications. In Sect. 4 we present an analytical treatment of the wind equations, which provides interesting constraints on the existence of such winds, as a function of the initial parameters. In Sect. 5 we briefly compare our results with those obtained by more complex hydrodynamical codes. Finally, in Sect. 6 we present our conclusions and outline future work.

2. Summary of previous results

The radiation force on a moderately ionized gas due to incident ultraviolet radiation is primarily via line absorption, rather than continuum electron scattering (CAK). In a constant velocity gas the 1000 times larger cross-sections of resonant line transitions over continuum Thomson scattering has little effect because the narrow wavelength ranges spanned by each transition contain relatively little UV continuum. However, a real wind, driven by a central radiation source will be accelerated, and so the wavelength for each absorption line will be Doppler shifted by the relative velocity of the gas with respect to the source. If the radial velocity gradient shifts the absorption wavelength sufficiently for each gas element, then fresh UV continuum is absorbed, leading to continued acceleration. As the process continues the fraction of the UV continuum that is absorbed is greatly increased. The absorption cross-section then becomes a *local* function of the physical conditions of the wind (the "Sobolev approximation", Sobolev 1960). CAK introduced a numerical "force multiplier", $M(t)$, which represents the enhancement of the radiation force due to line absorption with respect to pure electron scattering. $M(t)$ depends on only one local quantity, the "effective optical depth", t, defined as

$$t = \sigma_{\rm T} n v_{\rm th} \left| \frac{{\rm d}v_r}{{\rm d}r} \right|^{-1} \tag{1}$$

where $\sigma_{\rm T}$ is the Thomson cross section, n the gas density, $v_{\rm th}$ the thermal velocity in the gas, and $v_{\rm r}$ the radial component of the velocity.

Taking the thousands of, mostly weak, UV absorption lines for each ion into account, CAK estimated the following analytic power-law approximation for $M(t)$

$$M(t) = K \times t^{-\alpha} \tag{2}$$

where α is a positive number (with a typical value $\alpha = 0.6$) and K is 0.1–0.4.

However, as a gas becomes more ionized, either collisionally from an increased temperature, or through photoionization due to the intense UV source, the number of transitions available for absorption is reduced quite dramatically. In launching AGN winds this is a well known problem, and ad hoc schemes to shield the gas have been proposed (e.g. "hitchhiking gas", Murray & Chiang 1997).

A useful, second-order approximation, which takes the ionization state of the gas into account and solves the divergence of the previous equation for small t, is the following (Abbott 1986)

$$M(t) = K \times t^{-\alpha} \times \left[\frac{(1 + \tau_{\rm MAX})^{1-\alpha} - 1}{\tau_{\rm MAX}^{1-\alpha}} \right] \tag{3}$$

with $\tau_{\rm MAX} = t \times \eta_{\rm MAX}$, where $\eta_{\rm MAX}$ is a coefficient that is strongly dependent on the ionization parameter, ξ. This relation was studied by Stevens & Kallman (1986) who produced an analytic approximation that is correct within 10% over the whole range of interest for ξ. We plot this relation in Fig. 1, together with the dependence on ξ of the constant K. In a wind, ξ can be as high

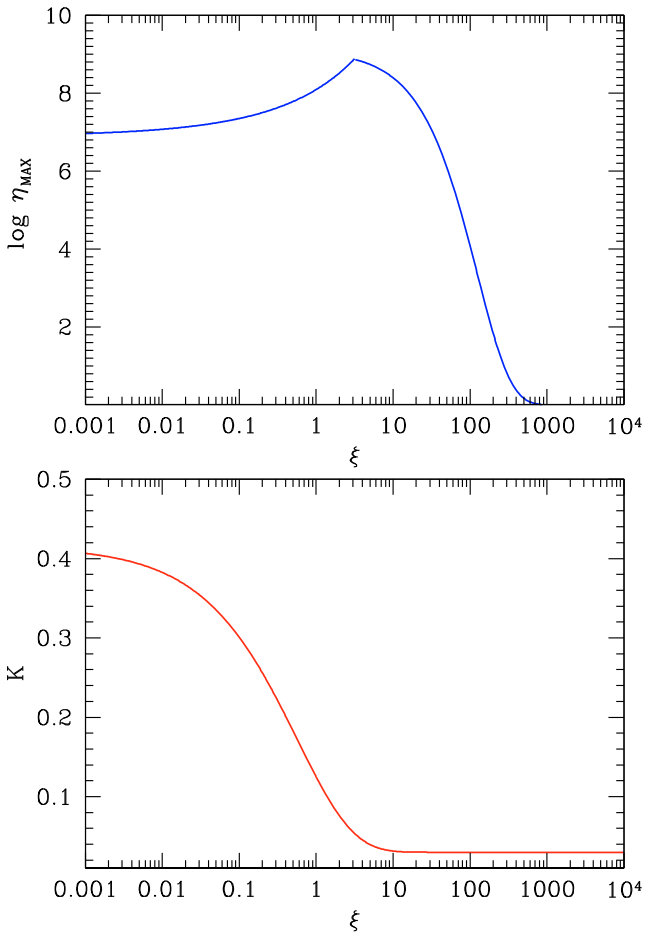

Fig. 1. Analytic approximation for the parameters K (solid line) and η_{MAX} (dashed line), as a function of ξ (Stevens & Kallman 1986).

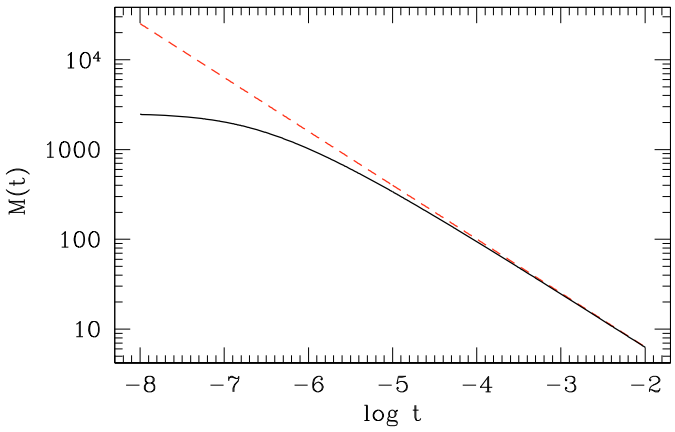

Fig. 2. Force multiplier $M(t)$ vs. optical depth t for a neutral gas in the CAK formulation (straight dashed line), and the Abbott (1982) and Stevens & Kallman (1986) formulation, that allow for ionization state and are more accurate for low effective optical depth ($t < 10^{-5}$).

as 10^3–10^4 at the inner surface, but then rapidly drops to low values ($\xi < 1$) because of the lowered X-ray flux. As a consequence, in the range of interest for a wind both η_{MAX} and K are constant to within a factor ~2. In Fig. 2 we plot Eqs. (2) and (3) for a neutral gas. We note that the correction factor is significant only if $t < 10^{-5}$.

Using these results, P00 developed a code which solves the hydrodynamical equations for a wind arising from an accretion disk, pushed by a central radiation force described by the above equations. In this work, a SS disk is assumed, and the ionization state is determined by the incident X-ray radiation from the central source. The main conclusion of P00 (in agreement with the previous work of Murray et al. 1995) is that a wind can easily arise from the accretion disk of AGN, under some initial conditions (SS disk, with a choice of free parameters such as the Eddington ratio and the X/UV ratio, which will be discussed in the next Sections). The dependence of the wind properties on the black hole mass and accretion efficiency is particularly interesting for they can now be tested against observations, as we discuss below. The black hole mass, M_{BH} and the accretion efficiency relative to Eddington, ϵ_{EDD}, are the parameters determining the luminosity of AGN.

3. Radiation-driven acceleration of a wind

Several physical effects need to be considered in the equations of the radiation force, to understand whether this external force is capable of accelerating the wind up to velocities of $\sim 10^4$ km s^{-1} or higher, as observed in BAL quasars.

The results summarized above (Sect. 2) show that a radiation-driven wind can arise from accretion disks in AGNs. However, the breadth of initial conditions that produce such a wind are at present unknown. First, while the SS disk is a plausible solution, many other disk structures are possible. Secondly, and more importantly, even within the SS disk paradigm the initial parameters are unknown: the black hole mass, the Eddington ratio, and the viscosity parameter $\alpha(disk)$. Finally, since the physical mechanism for the initial launching of a wind is not known, the radius at which the wind is launched is also unknown. However, recent studies of warm absorber winds in local AGNs suggest that winds on scales as small as a few thousand gravitational radii from the central black hole are possible (Krongold et al. 2006).

An important aspect of the solutions, found in the papers of Murray et al. (1995) and P00, is that the sonic and critical points of the wind are reached at a low height H above the disk with respect to the distance from the central source R ($H/R < 0.1$). Also, the velocities at the sonic and critical points are a few 100 km s^{-1}, which is only a few percent of the final BAL velocities ($\sim 10^4$ km s^{-1}).

As discussed briefly in the introduction, radiation pressure is expected to be relevant (and probably dominant) in the wind acceleration, regardless of the details of the launching mechanism. However, following the theory summarized in Sect. 2, in order for the absorption line mechanism to be effective, a balance between the intensity of the X-ray radiation (which determines the ionization parameter) and the intensity of the UV radiation (which provides the momentum needed by the gas to accelerate to high velocities) is required (Murray & Cheng 1995).

In this paper we discuss the general conditions for the acceleration of a line-driven wind after the launching phase. In particular we investigate whether the "thin wind" geometry proposed by Elvis (2000), which is successful in explaining a wide set of observational properties, can arise naturally. The main unexpected features of the Elvis (2000) geometry are that (1) the wind is thin ($\Delta R/R < 1$); and that (2) the wind is initially quasi-vertical, making a hollow cylinder of height $h/r \sim 1$, before becoming a radial, biconical flow.

3.1. The QWIND code

We developed the *QWIND* code with the following assumptions:

1. The X-ray source is point-like, isotropic and located at the center of the disk.
2. The UV/optical source is the accretion disk, emitting according to the SS model, which gives $R(UV) \sim 30\ R_S$. In our model the wind inner radius can be as small as $100\ R_S$, so the dimensions of the UV/optical source is non-negligible, and the disk cannot be considered a point source. Therefore, the dependence of the disk emissivity with radius, and the actual continuum emitting disk extent are included. We also take into account the anisotropy of the disk emission, which has important consequences for the wind properties. The radiation is zero on the disk plane, and increases with the cosine of the inclination angle of the disk with respect to the wind. Limb darkening (Fukue & Akizuki 2007), which would accentuate this effect, has been neglected.
3. The gas is launched from the disk at all radii between an inner radius $R_{\rm IN}$ and an outer radius $R_{\rm OUT}$, to a height H above the disk, with given density n, temperature T, and initial vertical velocity v_0. The radial velocity of this newly launched gas is zero, while the angular velocity in the disk plane is Keplerian.
4. The wind is subject only to the central gravitational force F_G due to the black hole of mass $M_{\rm BH}$ and radiation force F_r. Internal gas pressure is neglected, as is the gravity of the disk.
5. The radiation force in each element of the gas is computed using the CAK and Abbott (1986) equations described in Sect. 2 (Eqs. (2) and (3)). The ionization parameter, ξ, is determined assuming a cross-section $\sigma_X = 100\sigma_{\rm T}$ if $\xi < 10^5$, and $\sigma_X = \sigma_{\rm T}$ if $\xi > 10^5$. This simple approximation reflects the fact that when the ionization factor is too high, there are no bound electrons for photoelectric absorption to be effective. Below this critical value, photoelectric absorption on the electrons in the inner shells of metals is much more effective than Thomson scattering in removing X-ray photons. Using this approximation, if $\xi > 10^5$, X-rays penetrate deep into the wind, keeping ξ high, until the Thomson optical depth is higher than 1 ($N_{\rm H} > 1.5 \times 10^{24}$ cm^{-2}) or the R^2 factor makes ξ decrease below 10^5. Until this point, the radiation force is negligible because $M(t)$ is small. Deeper inside the wind, where $\tau_X > 1$, the UV radiation is also fully absorbed, and again $\sigma_X = \sigma_{\rm T}$, and therefore the radiation force will be negligible in this case too. If instead $\xi < 10^5$ the X-rays are absorbed in a thin layer[1] $N_{\rm H} \sim 10^{22}$ cm^{-2} and the ionization parameter drops as $\xi \propto e^{-100\sigma_{\rm T} N_{\rm H}}$, rapidly reaching the values at which the force multiplier becomes significantly higher than 1.

QWIND follows a gas element of radial thickness ΔR ($\Delta R \ll R$) from the accretion disk to radii greater than $10^3\ R_S$, starting from a set of initial radii $R_{\rm i}$[2]. This approach, consisting of following the trajectories of a fluid element, is similar to that adopted in several previous papers that analyze disk outflows (Icke et al. 1980; Tajima & Fukue 1996; Watarai & Fukue 1999). The acceleration of a gas element belonging to the ith stream line, at coordinates R, ϕ, z, is simply given by: $a = -GM_{\rm BH}R^{-2} + F_{\rm RAD}/m(R)$ where $m(R)$ is the mass of the gas element, calculated from the mass conservation equation (therefore depending on the radius and velocity of the gas element, and on the initial density profile). The radiation force $F_{\rm RAD}$ is estimated integrating the contribution of each disk element

$$F_{\rm RAD} = \int_{\rm DISK} f(\phi) {\rm e}^{-\tau} \frac{l}{4\pi R^2 c} \sigma_{\rm T} (M(t) + 1), \quad (4)$$

where $f(\phi)$ is the geometrical projection factor of each disk element as seen from the gas element; l is the luminosity of the disk element; $M(t)$ is the force multiplier, estimated as described above, and τ is the optical depth, estimated adding the contributions of the stream lines between the gas element and the disk: $\tau = \Sigma_i \sigma_i \times \Delta R_i \times n(R_i)/f(\phi)$, where $n(R_i)$ is the density of the gas element in the ith stream. The luminosity l of each disk element depends on the radial distance from the center of the disk, as estimated in a SS disk.

Our choice to integrate over the disk structure is motivated by the non-negligible dimensions of the disk with respect to the inner wind streams: in our computation the disk emission is calculated out to a radius of $400\ R_S$ (even if the contribution to the total luminosity is negligible for $R > 100\ R_S$), while the inner wind radius is $100\ R_S$ (see next section for further details on the computation domain).

The computation starts from the innermost stream line (free from absorption), and then proceeds to the outer ones. At each step, the calculations are done in the following order:

1. We estimate the absorption due to the inner stream lines. For the UV component, this is done simply adding the column densities of the inner stream lines, and multiplying by the Thomson cross-section. For the X-ray component, the computation is more complex: for each stream line crossed by the light ray from the disk element, we estimate the ionization factor and then, depending on its value, the X-ray cross section, following the prescription described above.
2. Using the absorption correction estimated in the previous point, and integrating over each disk element, we compute the flux on our wind element.
3. We estimate the density of the gas element from the values of density, mass and velocity of the previous computation step, and requiring mass conservation.
4. We estimate the force multiplier $M(t)$, following the prescription described in the 5th point of the code properties (above).
5. We obtain the acceleration on the gas element, and we compute the new spatial coordinates and velocity.

As a consistency check of the numerical stability of QWIND, we performed several runs with no radiation force contribution, and we checked that the evolution of the stream lines are those expected in a Keplerian problem. In particular, we checked that the conservation of angular momentum holds, and that the results are stable against changes in the number and dimensions of the gas elements used in the computation.

Neglecting the internal gas pressure makes the stream lines of gas in *QWIND* intersect unphysically. When two stream lines intersect, this means that the gas in the internal line is pushed outwards more than the gas on the external line. In reality this obviously cannot happen, and is prevented by the horizontal

[1] The situation can be complicated by the effects of secondary ionizations, which make ξ decrease more slowly than exponentially (Maloney et al. 1996). However, this effect is not important when ξ is high, and the external electrons (the targets for secondary ionizations) are already free.

[2] Note that throughout the paper $R_{\rm i}$ and $n - i$ refer to the initial radius and density, respectively, of the ith stream line, while $R_{\rm IN}$ and $n_{\rm IN}$ are the initial radius and density of the first stream line, i.e. $R_{\rm IN} = R_{\rm i}(i = 1)$, $n_{\rm IN} = n_{\rm i}(i = 1)$

component of the gas pressure. However, the two stream lines do delineate a limiting cone that a fully modeled wind must keep within. The gas pressure force between the two "lines" will make the gas move along a line whose inclination angle with respect to the disk axis is intermediate between the two lines computed by *QWIND*. This approximation therefore makes the results of *QWIND* usable only in this bounding sense, but should not change the general findings of interest, i.e. whether the wind can be accelerated by radiation pressure, the approximate angles to the disk, and covering factor of the central source, since these properties strongly affect the observables.

Another important effect neglected in our treatment is the change in momentum at the bending of the wind, which is expected to produce shocks and, possibly, soft X-ray emission, although this is unlikely to dominate the X-ray luminosity of the AGN. The case for the outflowing gas as a source of the soft X-ray excess observed in many quasars has been discussed by Pounds et al. (2003).

The number of stream lines used in the runs discussed in this paper is kept to just 20. We also made several runs with a larger number of lines (50), to check for discretization effects and found that the properties of the solutions do not change significantly.

The initial density of the wind at a radius R is one of the main free parameters of our model. In general, we parametrize the density as $n_{\rm i}(R_{\rm i}) = n_{\rm IN} \times (R_{\rm i}/R_{\rm IN})^{-\beta}$. Two particularly interesting cases are $\beta = 0$ (constant density at all radii) and $\beta = 15/8$, the density scaling in the SS disk. In this paper, we adopt $\beta = 0$ in our examples. Different cases (and, in particular, the SS disk-like profile, will be investigated in a forthcoming paper.

The initial vertical velocity v_0 is a free parameter of the code and is a few 100 km s^{-1}. This velocity is much lower than the escape velocity, therefore most of the kinetic energy needed to make a wind must be provided by the external radiation force.

With these assumptions, the total mass outflowing from the disk is easily derived, integrating the contribution from each disk ring. The fraction of this mass that falls back onto the disk versus the fraction which escapes through a wind, depends on the subsequent acceleration phase, and is studied by our model.

The initial parameters v_0 and $n_{\rm i}(R_{\rm i})$ are in reality a result of the previous launching phase. For example, in a purely radiation-driven wind, the mass loss rate is uniquely determined by the regularity and stability conditions at the "critical point" (CAK, Lamers & Cassinelli 1999; Murray et al. 1995). Since we are not studying this launching phase here, a fundamental requirement is that our final results do not depend critically on the exact values of these parameters. Since the density profile does affect the acceleration phase of the wind (because it determines, together with the X-ray flux, the ionization parameter), it is particularly important that the final results of the acceleration phase are independent of the exact value of the initial velocity, provided that it is small compared with the final velocity, and large enough to be supersonic (this, for temperatures of a few 10^6 K implies v_0 a few 10^2 km s^{-1}). As we discuss in detail below, we have carefully checked that this is indeed the case for our wind solutions, and that, for particular values of the initial velocity (inside the range mentioned above), our solutions satisfy the critical point conditions for a purely radiation-driven wind.

We next discuss the solutions obtained with our code *QWIND* for different choices of initial parameters. First, we concentrate on a particular "baseline" solution, in order to understand the physics of the wind. Then, in Sect. 3.3 we discuss the stability of our solutions. In Sect. 3.4 we discuss the dependence of the disk properties on the initial physical conditions.

Table 1. Baseline *QWIND* model parameters.

Parameter	Value
$R_{\rm IN}$	100 R_S
$R_{\rm OUT}$	800 R_S
v_0	10^7 cm s^{-1}
$\epsilon_{\rm EDD}$	0.5
$M_{\rm BH}$	2×10^8 $M_\odot$
$n_{\rm IN}$	2×10^8 cm^{-3}
β ($n_{\rm i}(R) = n_{\rm IN} \times (R_{\rm i}/R_{\rm IN})^{-\beta}$)	0
T	2×10^6 K
f_X	0.15

In Sect. 3.5 we briefly discuss a small survey of parameters in order to show the potential of our method in studying the wind properties in a variety of physical conditions.

A systematic analysis of all the variables, including different density profiles, and the effect of toroidal magnetic fields, will be the subject of a forthcoming paper.

3.2. Results: the baseline model, a case study

We show here the results obtained from running *QWIND* with the initial parameters given in Table 1. The inner and outer radii were chosen in order to investigate the region where a radiation-driven wind is expected, starting from an inner radius close to the outer UV-emitting region of the accretion disk, and studying the solutions up to an outer radius large enough to contain the inner broad line region. The initial velocity was arbitrarily chosen. The important points related to this parameter are: (a) its value must be small compared with the escape velocity; and (b) the exact initial value should not significantly affect the final results.

A further fundamental parameter in the model is the ratio between ionizing radiation and bolometric emission, f_X. Considering that the whole 0.1–100 keV spectrum contributes to the gas ionization, and that the wavelength range of the intrinsic disk emission is from optical to X-rays, a typical value for this ratio is $f_X \sim 15\%$ (e.g. Elvis et al. 1994; Risaliti & Elvis 2004). Quite different values are however possible, due to the large dispersion of the X-ray to optical ratio among quasars, and to its dependence on optical luminosity (e.g. Steffen et al. 2006; Young et al. 2010). We discuss the effects of changing this parameter in the next sections.

The main properties of the solutions are shown in Fig. 3. In the upper panel we show the wind lines in a plane perpendicular to the accretion disk. In the lower panel we show the ratio between the final velocity and the escape velocity for each wind line. By definition, we have a wind when the gas velocity becomes higher than the escape velocity, i.e. when the ratio in Fig. 3b grows to values greater than 1. In Fig. 4 we show the velocity profile and force multiplier $M(t)$ for the fifth stream line, i.e. the one reaching the highest final velocity.

Several interesting properties of the wind can be drawn from Figs. 3 and 4:

– *Initial distance*: Fig. 3b shows that the baseline model gas reaches escape velocity only if it is launched between ~150 R_S and ~250 R_S. At smaller radii, the gas is too ionized for the radiation force to be effective. At greater radii, the UV radiation is not sufficient to push the gas up to escape velocity. The exact values for the allowed radius range depends on the inner radius (in our case $R_{\rm IN} = 100\ R_S$). If, for example, $R_{\rm IN} = 300\ R_S$ (and all the other initial parameters are the same), it would be impossible to have a wind at $R = 300\ R_S$,

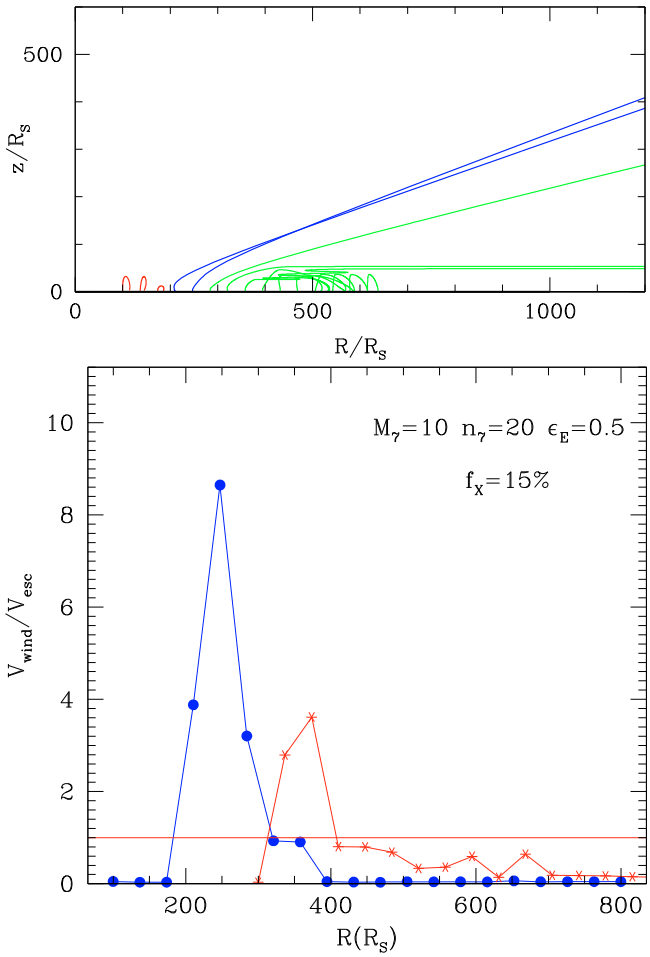

Fig. 3. Results of the simulations assuming a constant initial density profile. In this example, $R_{\rm IN} = 100\ R_S$, $R_{\rm OUT} = 800\ R_S$, $n_{\rm IN} = 2 \times 10^8$ cm^{-3}, $v_0 = 10^2$ km s^{-1}, $f_X = 15\%$, $\epsilon_{\rm EDD} = 0.5$, $M_7 = 20$. The *upper panel* shows the wind geometry. In the *lower panel* we plot the ratio between the final velocity of each stream line and its escape velocity, as a function of the initial radius. We also show the final velocity versus radius for a wind with the same initial parameters but a larger inner radius ($R_{\rm IN} = 300\ R_G$).

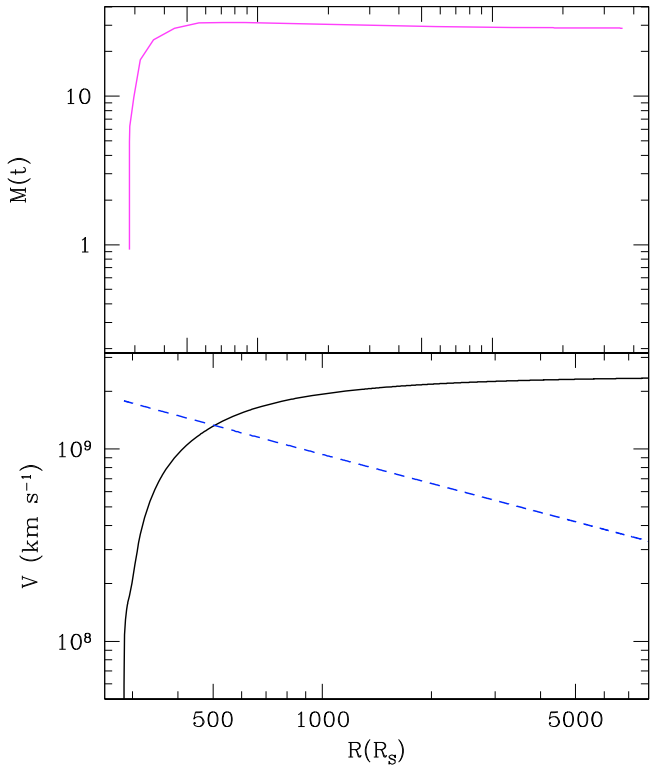

Fig. 4. Force multiplier, $M(t)$, (*upper plot*) and velocity (*lower plots*) versus radius for the fifth stream line in our case study. The dashed line in the lower plot represents the escape velocity as a function of the distance from the central black hole. See text for details.

because the gas is too ionized, due to the absence of shielding from the central X-ray emission. A wind at larger radii could however be possible, as we show in Fig. 3. *QWIND* modeling thus provides a simple explanation for the existence of a wind arising only from a narrow range of distances from the center.

– *Inner failed wind*: the inner stream lines form a "failed wind" that shields the outer stream lines from the central X-ray radiation. This shielding is fundamental to decreasing the ionization parameter in these stream lines, so allowing an effective radiative acceleration. This inner component fulfils the function of the "hitchhiking gas" invoked by Murray & Cheng (1995).
– *Radiation force*: the upper panel of Fig. 4 shows the profile of the force multiplier $M(t)$ for the fifth stream line in Fig. 5. Note that the maximum value is never higher than ~30. The relatively low values of $M(t)$ (well below the values >100 estimated by CAK in hot stars) imply that only fairly large values of $\dot{M}/\dot{M}_{\rm Edd}$ (>0.03) can produce an escaping wind.
A more technical consequence of the estimated values of $M(t)$ is that the correction factor in Eq. (3) is never important, and Eq. (2) is a good approximation of the force multiplier (Fig. 2, i.e. $\log t > -5$). This makes possible an analytic analysis of the wind launching problem, which we discuss in Sect. 4.
– *Velocity*: Fig. 4 (lower panel) shows the velocity profile for the fifth stream line of our case study. The acceleration is fast, and the escape velocity is reached at ~500 R_S. Then the velocity continues to slightly increase. In this phase the radiation force is still effective in supporting the wind against gravity. Indeed, the "effective" Eddington ratio, which depends on the actual one, $\epsilon_{\rm EDD}$, the force multiplier, and the inclination angle θ of the disk as seen from the wind line, is $\epsilon_{\rm EDD} \times M(t) \times \cos\theta > 1$ up to large radii ($R \sim 5000\ R_S$).
– *Geometry*: Fig. 3a shows that the gas rises vertically for ~50 R_S, and then bends toward a radial direction. Whether the gas falls down or maintains this direction depends on the effectiveness of the radiation force (see below). The angle of the wind above the disk is approximately 20 deg., giving a substantial covering factor of 35%. We note that the actual value of the covering angle is somewhat uncertain because the lines are treated as independent while, in reality, when two lines intersect, the gas pressure from the inner line pushes the gas on the outer line outwards, altering the final covering factor.

3.3. Check of initial conditions

In order to test the reliability of our initial conditions, in particular regarding the initial values of the vertical velocity and the height above the disk, we performed two checks:

1. We varied the initial height from $H = 5\ R_S$ to $H = 15\ R_S$, and the initial velocity from 100 to 300 km s^{-1}. No significant change in the final properties of the wind was found.

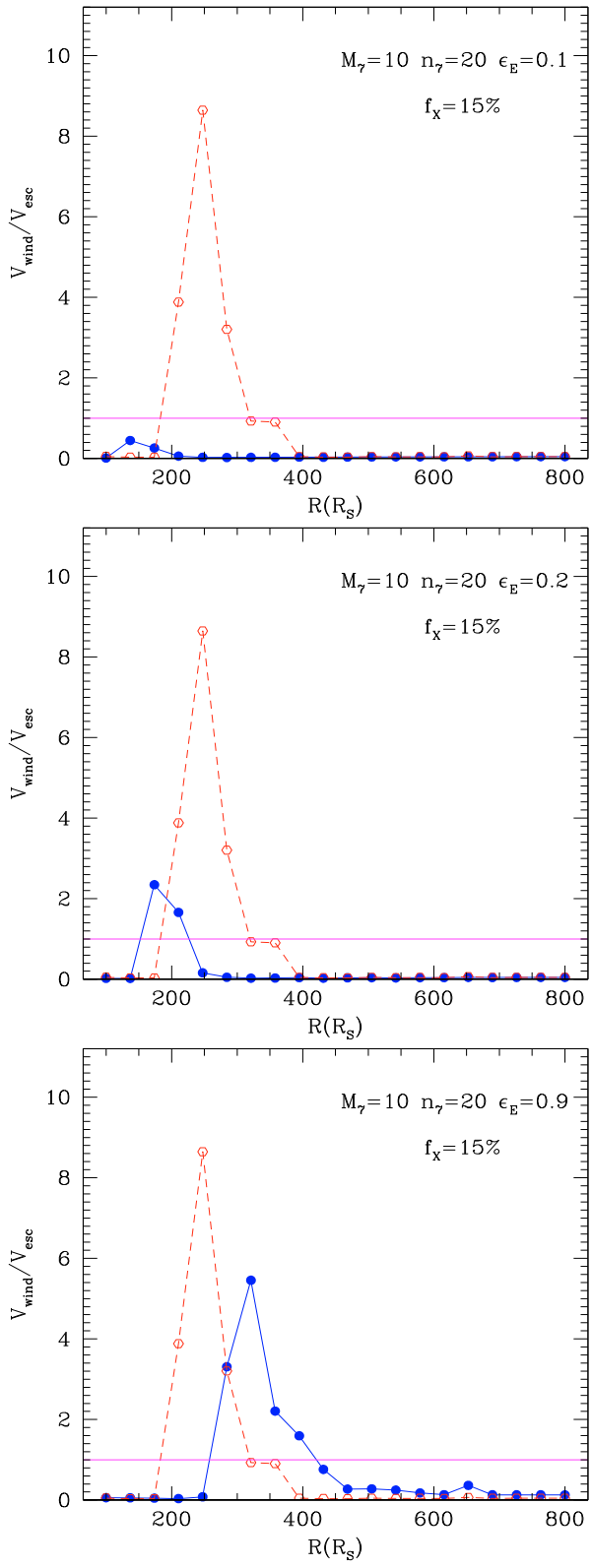

Fig. 5. Ratio between the gas final velocity and its escape velocity for several values of the Eddington ratio, ϵ_{EDD}. The red dashed line reproduces the same profile for the "case study" shown in Fig. 3.

2. We followed the wind streamlines backward in time down to the critical point (estimating this location as in Murray et al. 1995) and required that our solutions satisfy the regularity and stability conditions at the critical point (CAK). We iteratively varied the initial velocity until a consistent solution was found. A solution was found with a value of the initial velocity within our range of study (v_0 = 100–300 km s^{-1}).

The solution provided by *QWIND* thus represents the supersonic part of a purely radiation-driven wind (i.e. the case where, even in the subcritical phase, the radiation force is the only external force present in addition to gravity), and is in all respects equivalent to that found by Murray et al. 1995. The existence of such solutions within the range of initial velocities we are exploring shows that our approach is well justified, at least in the pure radiation-driven scenario.

3.4. Dependence on the individual parameters

In order to explore the dependence of our solutions on the initial parameters, we proceed in two steps: first, we analyze several cases close to the baseline model, changing the density, the X-ray to UV ratio, the Eddington ratio, and the black hole mass, in turn. Then, in the next subsection, we show the results of a survey of the $\epsilon_{EDD} - M_7$ space for a few choices of the other initial parameters to show the potential of our method for exploring the parameter space of initial conditions.

First, starting from the baseline model (Table 1), we systematically changed ϵ_{EDD}, f_x, n_8, M_{BH}, one at a time: in Figs. 5–8 we show plots analogous to that in Fig. 3b, i.e. the ratio between the final wind velocity and the escape velocity, v/v_{ESC}, against the initial wind radius[3]. From these results several additional indicators of the physical processes dominating the wind can be obtained, based on the dependence of v/v_{ESC} on the:

- *Eddington ratio* ϵ_{EDD} (Fig. 5): Too low a value (panel A, ϵ_{EDD} = 0.1) implies that the radiation is inadequate to accelerate the gas to escape velocity. With a higher value (panel B, ϵ_{EDD} = 0.2, a stream line is able to slightly exceed the escape velocity, thus forming a wind. Finally, for much higher values (panel C, ϵ_{EDD} = 0.9, to be compared with our case study with ϵ_{EDD} = 0.5) a wind is effectively launched, but at larger radii than in the previous cases. This is due to the higher X-ray luminosity, which over-ionizes the gas up to larger distances from the center.
  It is interesting to note that the maximum velocity reached by the wind in the case ϵ_{EDD} = 0.9 is less than in the baseline case of Fig. 3, despite the higher Eddington ratio. This is due to the reduction of the UV radiation pressure on the stream lines with the "right" ionization state, due to the higher distance. This result shows in a simple way that, due to the different dependences of the the physical conditions of the wind elements on the initial parameters, *a higher luminosity does not automatically imply a faster wind.* In our case, the intuitive increase of the wind velocity is observed increasing the Eddington ratio from 0.2 to 0.5, but not with the further increase to 0.9.
- *Density of the gas,* n_7 (Fig. 6): At low values of the density (left plot, n_7 = 3, c.f. n_7 = 20 in the standard case), the gas is overionized even at large radii, and it is therefore impossible to launch a wind. Increasing the density (n_7 = 10, right plot) the ionization parameter, ξ, decreases, making it easier to push the gas effectively through the line-absorption driven force. An even higher density shifts the wind towards inner radii, because the over-ionization region is limited to a smaller region.

[3] In these figures, and in the next sections, we adopt the convention $n_7 = n/(10^7$ cm$^{-3})$, $M_8 = M_{BH}/(10^8\ M_\odot)$.

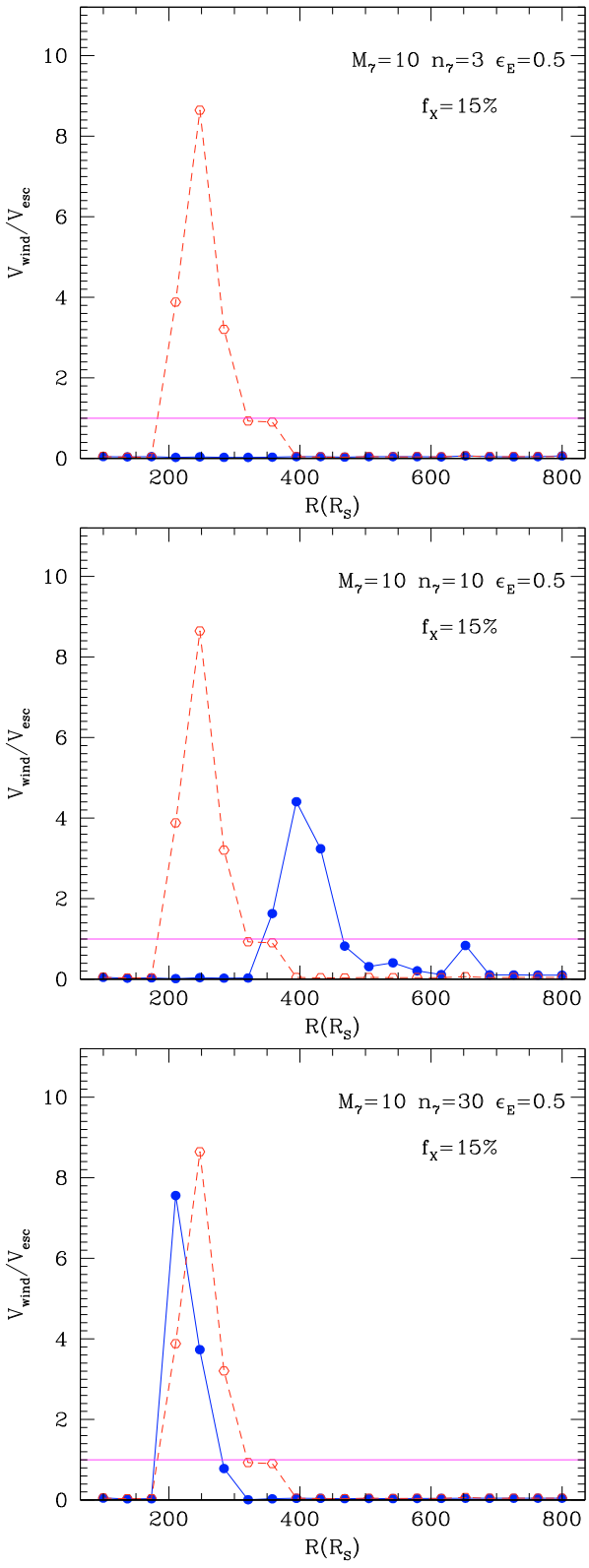

Fig. 6. Ratio between the gas final velocity and its escape velocity for several values of the initial gas density, $n_{\rm IN}$. The red dashed line reproduces the same profile for the "case study" shown in Fig. 3.

– *The ratio* f_X between X-ray and disk radiation (Fig. 7): Too high a value of f_X (in our example, $f_X = 25\%$, corresponding to a 2 keV to 2500 Å slope of $\alpha_{\rm OX} = 1.3$) produces a higher ionization parameter, and makes it more difficult to accelerate the gas. Lower values ($f_X = 5\%$, $f_X = 10\%$, corresponding to $\alpha_{\rm OX} = 1.6$ and $\alpha_{\rm OX} = 1.5$, respectively) mean a smaller ionizing continuum, and therefore a lower ionization factor for the inner gas of the wind, which can be accelerated up to the escape velocity. This effect was first noted by Murray & Chiang (1995).

– *Black hole mass* (Fig. 8): The wind properties strongly depend on the black hole mass. The dependence is quite complex, since the different physical parameters (ionization state, UV flux, disk temperature) scale in different ways with the black hole mass. Varying the black hole mass and leaving the other parameters as in our case study, we see that the higher the mass, the closer in is the wind. For the highest mass value ($M_{\rm BH} = 10^9\ M_\odot$) no wind is launched with the adopted choice of the initial parameters. The main physical driver of this behavior is the ionization parameter, $\xi \propto L/R^2$. Since $L \propto M_{\rm BH}$ (for a fixed $\epsilon_{\rm EDD}$) and the distance in physical units is $R \propto M_{\rm BH}$ (for a fixed value in units of R_S), the ionization parameter at a given distance in units of R_S decreases with $M_{\rm BH}$. The distance (in units of R_S) at which we have the "right", wind-producing, balance between ionization state and UV irradiation therefore decreases with increasing black hole mass, reaching values lower than our inner radius for $M_{\rm BH} = 10^9\ M_\odot$. In this case, it may be possible to obtain a wind from radii $R < R_{\rm IN}$. This scenario will be studied in a broader analysis of the parameter space, which will be presented in a forthcoming paper. Here we only note that this result does not imply that a wind is impossible at high masses: an example of wind from a $10^9\ M_\odot$ black hole is presented in the next section, where we show that a different choice of the initial density leads to higher ionization parameters, shifting the "wind zone" towards higher radii. In particular, we show that an initial value of the density $N_7 = 1$ (i.e. 20 times lower than our baseline case) implies that a wind can be launched *only* with black hole masses on the order of $10^9\ M_\odot$.

3.5. Parameter survey

In order to test the ability of *QWIND* to perform complete surveys of the parameter space, we ran a grid of 11×10 models, adopting the parameters of our baseline study, and varying the black hole mass and the Eddington ratio in the range 10^7–$10^9\ M_\odot$ and 0.1–1, respectively. The result is shown in Fig. 9. The allowed region for the wind launching extends down to $\epsilon_{\rm EDD} \sim 0.2$, showing that a radiation-driven wind is possible at luminosities much below the Eddington limit (as was also shown, in more detail, for a single case in Fig. 5b). Clearly, in these cases the enhancement of the radiation force due to line absorption plays a fundamental role.

As a further example of the application of *QWIND* we also tested the scenario of a hot, low density wind with a less substantial mass outflow. To test this, we run a *QWIND* grid analogous to the one described above, but with an initial density 20 times lower ($n_{\rm IN} = 10^7\ {\rm cm}^{-3}$). The results are shown in Fig. 10. In general, too low a density implies a too high ionization, and the wind cannot be launched. The situation is different only at very high masses, where the distances from the central source are large enough to provide the requested balance between ionization parameter and intensity of the UV source.

4. Analytic approximations

Since our main aim is to understand which physical conditions allow wind acceleration, we can search for further

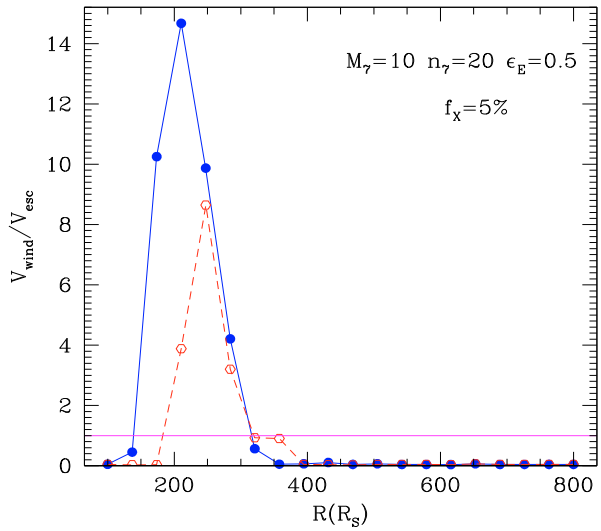

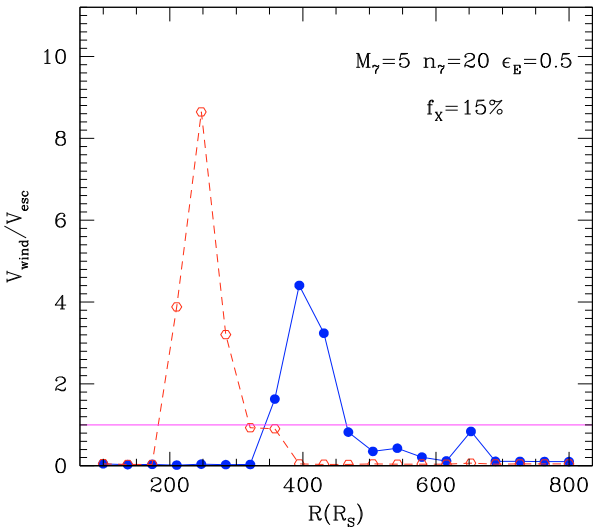

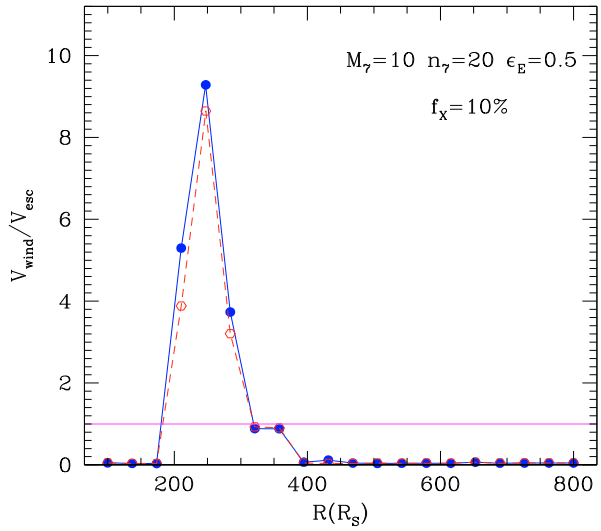

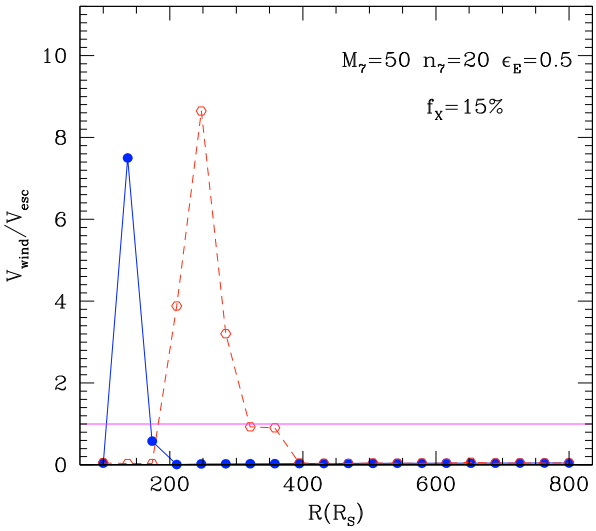

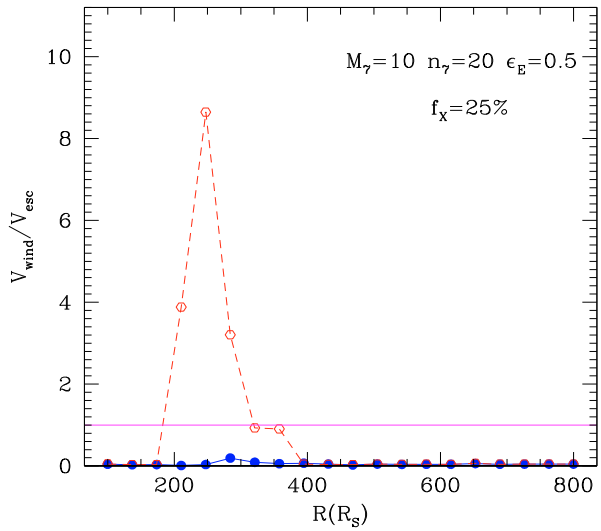

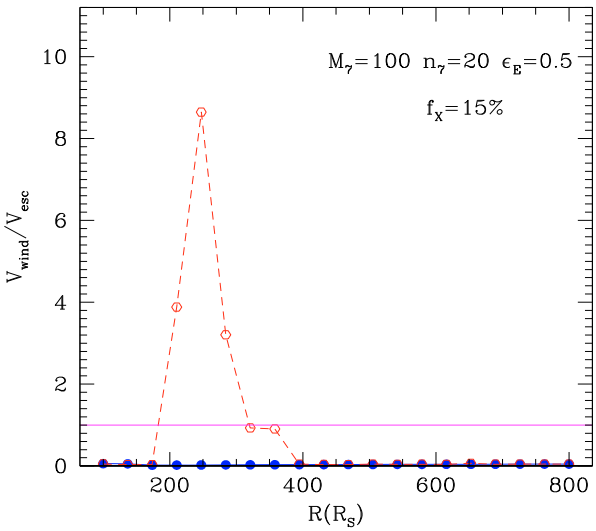

Fig. 7. Ratio between the gas final velocity and its escape velocity for several values of the ratio f_X between the X-ray and UV flux. The red dashed line reproduces the same profile for the "case study" shown in Fig. 3.

Fig. 8. Ratio between the gas final velocity and its escape velocity for several values of the central black hole mass, $M_{\rm BH}$. The red dashed line reproduces the same profile for the "case study" shown in Fig. 3.

simplifications which allow an even simpler treatment, based on an analytic model. Our aim here is not to study the details of the wind solutions, but rather to explore the parameter space in order to understand which are the initial conditions required in order to have accelerations up to several thousand km s^{-1}. The analytic treatment lets us search for the existence of wind solutions by finding regions of parameter space that satisfy two conditions: (1) that the final velocity exceeds the escape velocity; and (2) that the gas must not be overionized.

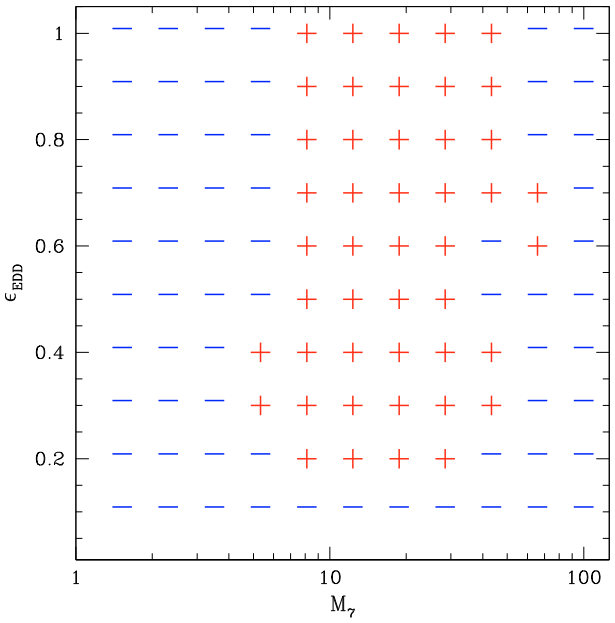

Fig. 9. Results of a survey of the $\epsilon_{EDD} - M_{BH}$ plane, with the other initial parameters equal to those of the baseline model. The "+" indicate that a wind is launched.

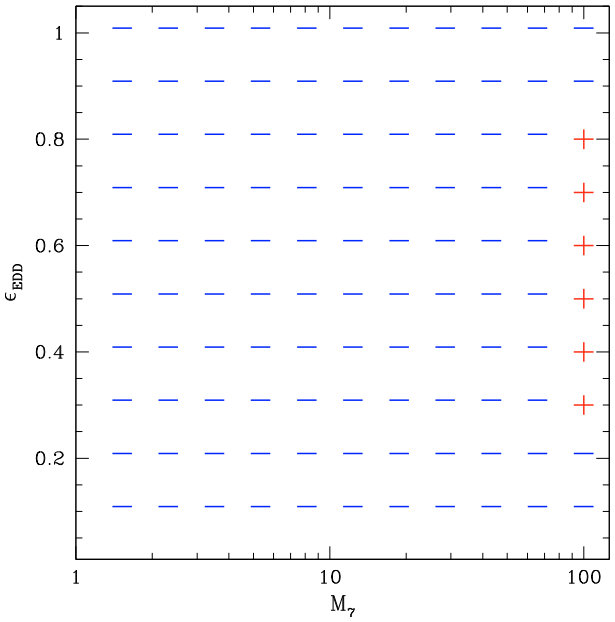

Fig. 10. Results of a survey of the $\epsilon_{EDD} - M_{BH}$ plane, with an initial gas density $n_{IN} = 10^7$ cm^{-3}, 1/20 of the baseline value. The "+" indicate that a wind is launched.

In this section we will make three extra approximations to the dynamical equations of the wind, which allow the equation of motion to be integrated analytically, so that the final velocity can be calculated directly. The approximations are:

1. An energy source with a constant inclination with respect to the wind. For the X-rays, this is the same as assumed in *QWIND* (spherically symmetric emission). For the UV, this is equivalent to the assumption of a fixed inclination angle of the wind stream lines.
2. Neglect of the gravitational term in the dynamic equation as, once the line-driven acceleration mechanism becomes effective, it usually dominates the gravitational term by a factor of 10 or more (see Sect. 4.3).
3. Line driving is well-reproduced by the simple equation $M(t) = K \times t^{-\alpha}$, which is valid only when the wind is not overionized, but we require a low ionization parameter as a condition for the acceleration of the wind (see below).

Each of these three approximations makes wind solutions more likely: (1) the spherical approximation implies that the UV radiation is not decreased by the geometrical projection factor of the disk; (2) neglecting the gravitational term obviously favors fast outflows; and (3) the force multiplier assumption maximizes the effect of line-driving. As a consequence we will obtain wind solutions in larger regions of the parameter space than found using the more precise numerical approach described in Sect. 3. We will show that in practice the analytically allowed parameter space is close enough to the results of the numerical code to make the analytical results useful in delimiting large regions of the multi-dimensional initial parameter space where it is *not* possible to accelerate a wind.

We discuss the third assumption in the next subsection. The integration of the equation of motion, and the condition on the final velocity are discussed in Sect. 4.2. We then show the results for a limited set of initial parameters, and, finally, we compare our results with those obtained with *QWIND*.

4.1. Relation between M(t) and ξ

Here we show that the equation of the force multiplier, $M(t)$ can be simplified into two regimes, depending on the ionization factor: $\xi < 100 : M(t) = Kt^{-\alpha}, \xi > 100 : M(t) = 0$. We then discuss the equation describing the motion of a gas element inside the wind.

In order to estimate the range of values of t for which the correction factor of $M(t)$ becomes important, and therefore $M(t)$ saturates to its asymptotic limit, we expand Eq. (3) for small t, obtaining

$$M(t) \sim K(1-\alpha)\eta_{MAX}^{\alpha}(1-\alpha\eta_{MAX}t). \quad (5)$$

This shows that in order to have $M(t) \rightarrow (1-\alpha)\eta_{MAX}^{\alpha}$ the effective optical depth must be

$$t \ll \frac{1}{\alpha\eta_{MAX}} \cdot \quad (6)$$

From Fig. 1 , for $\xi < 100$ this implies $t < 10^{-6}$. This condition can also be easily obtained from Fig. 2. For an outflowing wind reaching a radial velocity of $\sim 10^4$ km s^{-1} in a distance of 10^{16}–10^{17} cm, typical AGN values, we have an average $\frac{dv_r}{dr} \sim 10^{-7}$–$10^{-8}$ s^{-1} and so, from Eq. (1), $t \sim 7 \times 10^{-3}\ T_6^{0.5} n_8$, where $T = 10^6 T_6$ K and $n = 10^8 n_8$ cm^{-3}. It is easily seen from Fig. 1 that if the ionization factor ξ is lower than 100, $M(t)$ is never close to the saturation regime for reasonable values of the density and temperature, and $M(t) = K \times t^{-\alpha}$ is a good approximation. K is constant within a factor $\sim$2 in the range of interest (Fig. 1).

If $\xi > 100$ the situation is completely different, since it is obvious from Fig. 1 that the line absorption becomes negligible compared with electron scattering, and in this condition no wind can be launched unless the luminosity is super-Eddington. This is why the wind models of Murray & Chiang (1997) require additional, "hitchhiking" gas, to shield the gas that was to be accelerated, reducing ξ. Therefore, in the following we shall assume $\xi < 100$ in studying the dependence of the wind

from the other parameters. Now let us consider a gas element in the outflow at radial distance R from the center. The gas element is subject to gravitational force, $F_G = GM_{\rm BH}m_pR^{-2}$, and to the radiation force, $F_r = L(4\pi R^2c)^{-1}\sigma_{\rm T}(M(t)+1)$. The force multiplier $M(t)$ is given by Eq. (3), and depends on the density profile of the gas making up the wind. We assume a profile $n_{\rm i}(R) = n_{\rm IN}\times(R/R_{\rm IN})^{-\beta}$, as in our numeric code.

The flux at a given gas element inside the wind is given by $FL_0/(4\pi R^2)\times A(R)$, where L_0 is the intrinsic disk luminosity, F is the geometrical factor due the disk inclination (which is assumed to be constant in this analytical treatment) and $A(R)$ takes into account the absorption between the gas element under consideration and the luminosity source. While a detailed treatment of the absorption term would require a complete solution of hydrodynamical and radiative transfer equations, we can make some useful approximations:

- That the inner part of the gas is able to reach high enough above the disk that it shields the gas farther out. This assumption is supported by the results of *QWIND* (Sect. 3), and has the same effect as the assumption of hitchhiking gas by Murray & Chiang (1995).
- That each ring of gas with thickness ΔR contributes to radiation absorption with a column density of $\sim n\Delta R$. This is obviously a lower limit, since the wind is not perpendicular to the central radiation. However, the correction is small and can be neglected.

With these two assumptions, the absorption term can be written as

$$A(R) = {\rm e}^{-\sigma_{\rm T}\int_{R_{\rm IN}}^{R} n(R'){\rm d}R'} \tag{7}$$

where $\sigma_{\rm T}$ is the Thomson cross section. Assuming the same density profile as in our numeric code, $n(R) = n_{\rm IN}\times(R/R_{\rm IN})^{-\beta}$, we have

$$A(R) = {\rm e}^{-\frac{0.02}{\beta-1}\, n_8\, R_{100} M_7\left[1-\left(\frac{R}{R_{\rm IN}}\right)^{1-\beta}\right]}. \tag{8}$$

We can now write the equation of motion for the gas, simply requiring that the force on a gas element is equal to the difference between the external radiation force and the gravitational force. As in the *QWIND* code (Sect. 3), we neglect the internal pressure term, since we want to discuss the motion of the ion in the supersonic part of the wind, where gas pressure cannot affect the dynamics significantly. Furthermore, we assume that only radial forces are present. This implies the conservation of angular momentum, and a decoupling of the radial and tangential equations. The radial equation of motion can then be written, putting $\epsilon_{\rm EDD}$ for the Eddington ratio and $R_{\rm IN}$ for the initial radius, as

$$v_R\frac{{\rm d}v_R}{{\rm d}R} = \Phi_{\rm RAD} + \Phi_{\rm GRAV} \tag{9}$$

where the lefthand side gives the radial acceleration, while the righthand side is made up of two terms:

1. The line-enhanced radiation force, given by the flux multiplied by the force multiplier $M(t)$, and by a geometrical factor, $F(\phi)$, dependent on the inclination angle ϕ of the disk with respect to the gas element

$$\Phi_{\rm RAD} = \frac{GM}{R^2}\epsilon_{\rm EDD}A(R)F(\phi)K\left(nv_{\rm TH}\sigma_{\rm T}\left|\frac{{\rm d}v_R}{{\rm d}R}\right|^{-1}\right)^{-\alpha}. \tag{10}$$

2. The gravitational force, corrected by a factor $(1-\frac{R_{\rm i}}{R})$, obtained from angular momentum conservation, assuming that the gas element moves with the Keplerian velocity at the initial radius $R_{\rm i}$, and decreased by the continuum radiation force, due to Thomson scattering):

$$\Phi_{\rm GRAV} = -\frac{GM}{R^2}\left(1-\frac{R_{\rm i}}{R}\right)(1-\epsilon_{\rm EDD}F(\phi)A(R)). \tag{11}$$

A further fundamental condition is given by the mass conservation condition, $\dot{M} = 4\pi R^2 nv = {\rm const}$, which implies that the only stable solutions are those through the critical point, as first discussed by CAK75 and, in a context similar to ours, by Murray & Chiang (1995). (See also Lamers & Cassinelli 1999, for a textbook treatment.)

In general, Eq. (11) can only be solved using numerical codes. However, in our case we are interested in some special situations. In particular, the wind solution we are seeking is characterized by a sudden and strong radial acceleration (as demonstrated by the results of *QWIND* shown in Sect. 3), which changes the gas motion from slow and quasi-vertical to radial and fast (with velocity higher than the escape velocity). We can assume that in this accelerating phase the external force is dominant with respect to the gravitational term, which can be neglected. We also require that the final wind velocity, v_F, exceeds the escape velocity, $v_{\rm ESC} = \sqrt{2\,{\rm GMR}^{-1}}$, within a distance from the center of a few $10^3\ R_S$. We will then check whether our solutions fulfill the conditions described above. This consistency check will only show whether our wind solutions are acceptable, but allows that other solutions are possible. For example, we expect that, for a large set of initial conditions, the gas, after initially rising, will fall back onto the disk. (In these cases the gravitational term is obviously not negligible).

Neglecting the gravitational term, and requiring mass conservation, we obtain

$$R^2v_R\frac{{\rm d}v_R}{{\rm d}R} = \eta\left[R^2v_R\frac{{\rm d}v_R}{{\rm d}R}\right]^{\alpha} \tag{12}$$

where

$$\eta = (v_{\rm TH}\sigma_{\rm T}v_{\rm i}n_{\rm i}R_{\rm i}^2)^{-\alpha}KF(\phi)A(R)GM\epsilon_{\rm EDD}. \tag{13}$$

Since we are studying solutions with rapid radial accelerations, which quickly make the gas motion radial, we can assume that the geometrical factor is constant ($F(\phi) = F_0$). Furthermore, we neglect the dependence of $A(R)$ on the distance R, assuming $A(R) = A(1.2\ R_{\rm i})$. This approximation is reasonable, considering that our simulations with *QWIND* (Sect. 3) show that when a wind is successfully launched, the escape velocity is reached at a distance from the center $R_{\rm ESC}$ only slightly larger (by on average ~20%, from Figs. 5–8) than the initial distance of the stream line, $R_{\rm i}$. With these assumptions, Eq. (12) can be easily integrated between an initial radius, $R_{\rm i}$, and a final radius, R_F. The condition $v_F > v_E$ can then be written as

$$\eta^{\frac{1}{1-\alpha}}r_{\rm i}^{-1}\left[1-\frac{R_{\rm i}}{R_F}\right] > GMR_F^{-1}\,. \tag{14}$$

Finally, we adopt the initial density profile discussed above, and we assume $R_F = 2R_{\rm i}$. A choice of R_F is needed in our treatment, because having neglected the gravitational term implies that the above equation is always satisfied for $R_F\to\infty$. We assume $R_F = 2R_{\rm i}$, which, based on the above considerations on $R_{\rm ESC}$, is a rather conservative assumption (in all the cases analyzed with *QWIND* we found $R_{\rm ESC} < 2R_{\rm i}$), in the sense of allowing a larger parameter space for wind launching than in our

analytic treatment. This agree with our general approach, as discussed at the beginning of the present section.

We can then rewrite the above equation as:

$$\left[v_{\rm TH}\sigma_{\rm T}v_I n_I R_{\rm i}^2 (GM)^{-1})\right]^{-\alpha} kF_0 A\epsilon{\rm EDD} > 1. \quad (15)$$

Finally, adopting a proper parametrization for the physical quantities and substituting the numerical values for the constants, and assuming $\alpha = 0.6$, we obtain:

$$\epsilon_{\rm EDD} > 1.1\times10^{-3}A^{-1}F_0^{-1}\left[\sqrt{T_7}v_7 n_8 R_{\rm i,100}^2 M_7^{-1}\right]^{0.6}. \quad (16)$$

This condition, when combined with the requirement that the gas not be over-ionized (Sect. 4.2), will allow us to put on the wind-like solutions in a black hole mass – Eddington ratio plane, as we show in Sect. 4.3.

4.2. Effects of X-ray absorption

If the inner part of the wind is too close to the X-ray source, an over-ionization problem arises. An approximate treatment can be obtained by considering the X-ray cross-section of the wind gas as in P00. Using the approximation described in Sect. 3, a fundamental requirement for a radiation-driven wind to be launched is that $\xi = L/(n(R)R^2) < 10^5$, where L is the ionizing radiation. Adopting the same parametrizations as in the previous subsection, the above condition can be written as

$$1.5\times10^8 f_X n_8^{-1} R_{100}^{-2} M_7^{-1} A(R)\epsilon_{\rm EDD} < 10^5 \quad (17)$$

where $A(R)$ is the unabsorbed fraction of the X-ray radiation, and is given by Eq. (8), the cross-section being the same (for $\xi > 10^5$) as for the UV disk radiation. (Recalling that f_X is the fraction of the bolometric luminosity emitted in the X-rays.) In the work of Stevens & Kallman (1986) the objects considered as sources of radiation-driven winds were X-ray binaries, with a rather hard spectrum. As a consequence, only photons with $E > 1$ keV were taken into account in their estimate of the ionization parameter.

In our case, the typical intrinsic X-ray spectrum of an AGN is dominated by soft emission in the 0.1–1 keV band, which gives a significant – if not dominant – contribution to the ionization parameter. Therefore, we calculate the ionization parameter using the luminosity above 0.1 keV. As a standard value we assume that of Elvis et al. (1994), where the 0.1–100 keV luminosity is ~15% of the total (i.e. optical-UV-X-ray) emission of an AGN.

Assuming the density profile of the SS disk $n(R) = n_{\rm IN}\times(R/R_{\rm IN})^{-\beta}$ Eq. (17) can be finally rewritten as

$$\epsilon_{\rm EDD} < 0.0044\left(\frac{f_X}{0.15}\right)^{-1} M_7 n_8 \left(\frac{R}{R_{\rm IN}}\right)^{-\beta} A(R)^{-1}R_{100}^2\,. \quad (18)$$

4.3. Analytical results

The constraints from Eqs. (16) and (18) delimit the region of the black hole mass, Eddington ratio ($M_{\rm BH}, \epsilon_{\rm EDD}$) parameter space in which an outflowing wind can arise.

We can use Eqs. (16) and (18) to plot the allowed wind-launching regions in the $\epsilon_{\rm EDD} - M_{\rm BH}$ plane. Since Eq. (18) depends on the initial radius of each streamline, for a given set of initial parameters (wind inner radius $R_{\rm IN}$, density at the inner radius $R_{\rm IN}$, gas temperature T and X-ray to optical/UV ratio f_X) we compute the allowed region for each single streamline, and then we plot the convolution of all these regions. In this way, the meaning of the "analytic parameter surveys" are analogous to those plotted in Figs. 9 and 10.

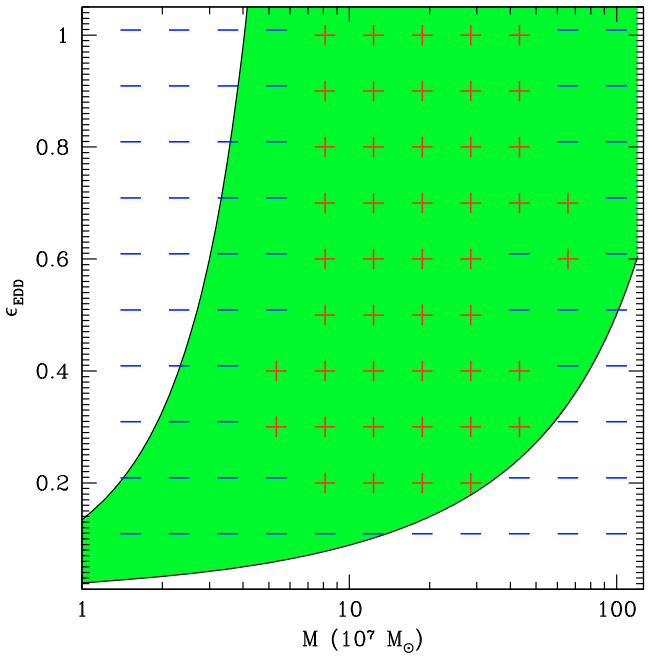

Fig. 11. Results of our numerical analysis for our baseline set of parameters. The green (shaded) region indicates where a wind can be launched. The analytic estimate is compared with the numerical result obtained with a *QWIND* survey.

We assume a baseline set of initial parameters (Table 1), as used in Eqs. (16) and (18): f_X =15%, $T = 2\times10^6$ K, $n_{\rm IN} = 10^8$ cm^{-3} at $R_{\rm IN} = 100\ R_S$. These parameter values are those required for the gas responsible for the observed UV and X-ray "Warm absorber" absorption lines (Nicastro et al. 1999; Netzer et al. 2002; Krongold et al. 2003) in quasar spectra. They are also the physical conditions needed for a gas confining the BEL clouds (which have $n \sim 10^{10}$ cm^{-3} and $T \sim 10^4$ K, Osterbrock 1989) as noted by Turner et al. (1994) and Elvis (2000).

Figure 11 shows the allowed ($M_{\rm BH}, \epsilon_{\rm EDD}$) parameter space for the baseline parameters, superimposed to the results of *QWIND* for the same set of parameters (already shown in Fig. 9. The two interesting results emerging from this plot are:

(1) The allowed region based on our analytic approximation is larger than obtained with the more detailed approach based on *QWIND*. This confirms that our approximations do not miss any possible wind solution, in agreement with our expectations (Sect. 4.1).
(2) The results of the analytic approximations are useful to exclude a significant part of the parameter space where a wind cannot exist. This approach can then be used for a genaral exploration of the parameter space, leaving the more time-consuming numerical approach for a smaller set of parameters. This was not obvious a priori, since too strong an approximation could have led to an too large (and therefore useless) allowed region.

While a complete investigation of the parameter space is not the purpose of the present work, it is useful to show the results of the analytic approach for a small set of initial parameters, as examples of the possible uses of this technique.

We show in Fig. 12 the allowed regions in four cases, obtained from the baseline case changing one or two initial parameters, in order to test four different physical situations:

(a) BELR wind: It is interesting to investigate whether BEL gas could be accelerated directly by the radiation force.

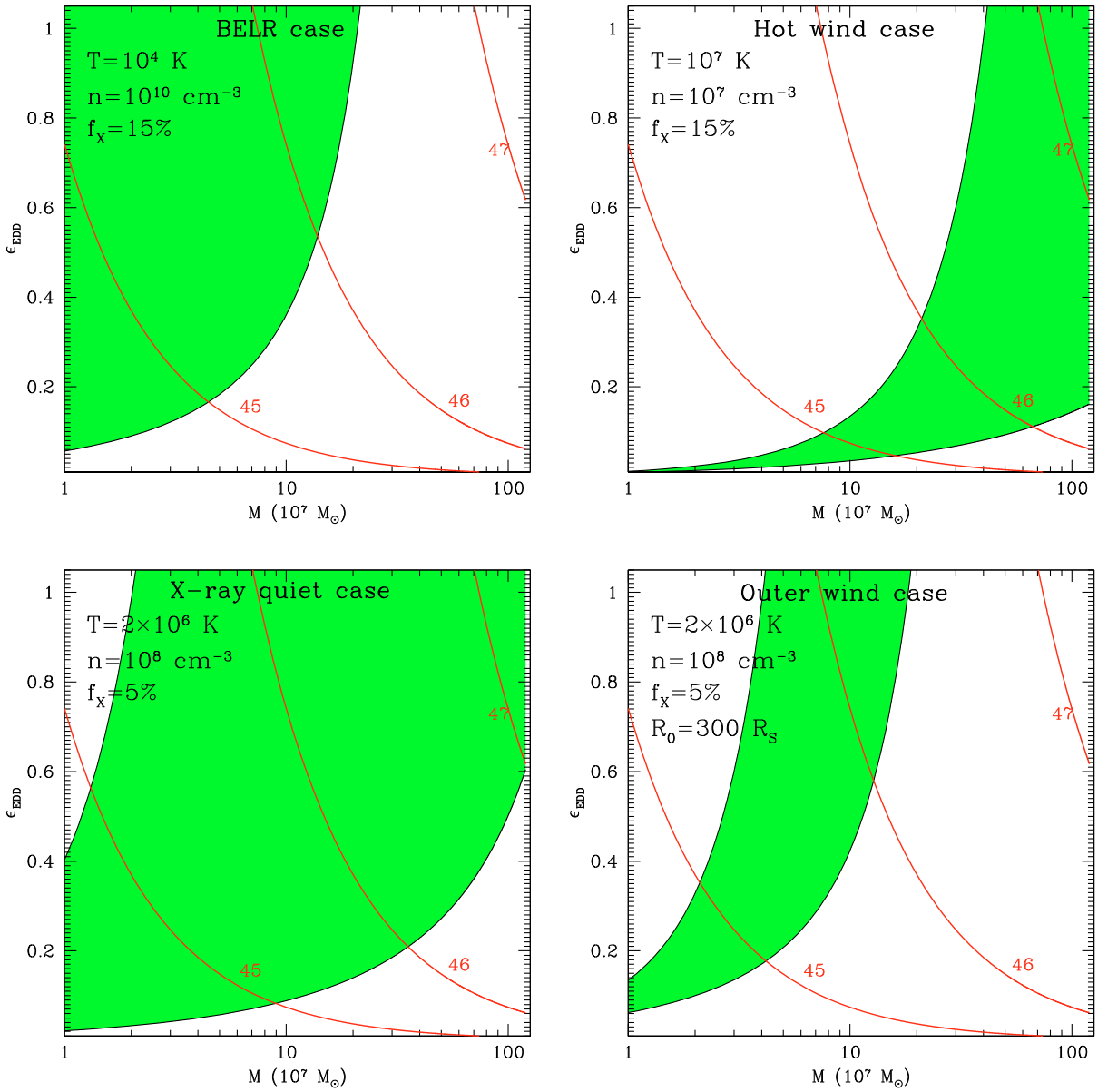

Fig. 12. Results of our numerical analysis for several choices of the initial parameters. The red lines show the total luminosity of the source. The green (shaded) regions are those allowed for wind launching. *Upper left panel*: BELR case; *upper right panel*: hot wind case; *lower left panel*: wind from an X-ray quiet source; *lower right panel*: wind with a large inner radius ($R_{\rm IN}$ = 300 R_G).

Figure 12a shows that BEL gas cannot be accelerated to high velocities by the radiation force, except at relatively low mass black holes ($M_7 < 10$) and high Eddington ratios (except at the lowest masses). The physical reason is that in an overly dense gas the Doppler shift due to the radial acceleration is insufficient move the transition to fresh UV continuum, so the gas becomes self-shielded against line absorption. Thus in a too dense gas the effective optical depth, t, is never small enough to make the force multiplier $M(t)$ much higher than 1, for reasonable values of the radial velocity gradient ($\frac{dv_r}{dr} > 10^{-6}$ s^{-1}).
We stress that this result does not imply that a wind containing a cold and dense phase is possible only at low masses. Indeed, if the BEL gas is confined by a hot wind, it is expected that the pressure of the warm gas would drive them to similar velocities. However, a more detailed study is needed to test this statement. Here we note only that, in a wind like the one described in Elvis (2000), most of the kinetic energy is in the warm phase (80–90%). Therefore, from an energetic point of view it is likely that the dynamics of the whole wind (comprised of the cold phase, i.e. the BEL gas, and the warm phase) is determined by the warm phase.
(b) Hot wind: Fig. 12b shows the allowed region for a hot, low density wind. Only at the highest masses can such a wind be launched, because of the over-ionization due the low wind density. The ionization parameter of the wind decreases at high BH masses because in our scheme the distance of the stream lines is always the same in units of R_S. Therefore, increasing the BH mass implies a linear increase of the luminosity (at a given $\epsilon_{\rm EDD}$) and a quadratic increase of the physical distance, resulting in a linear decrease of the ionization parameter with $M_{\rm BH}$.
We note that this case is the same as in the second *QWIND* survey (Fig. 10). Again, the allowed region obtained with the

analytic approach is larger than that predicted with *QWIND* (Fig. 10).

(c) X-ray weak source: The fraction of the bolometric luminosity emitted in the X-rays, f_X, is important in the determination of the allowed region for a wind. The value used in the standard parameters set, $f_X = 15\%$, agrees with the observed spectral energy distributions (SEDs) of PG quasars (Elvis et al. 1994; Laor et al. 1997). However f_X depends on luminosity (Zamorani et al. 1981; Yuan et al. 1998; Steffen et al. 2006; Young et al. 2010) and values of ∼20–25% are found in nearby Seyfert galaxies. High values are also found in radio-loud quasars; in this case however beaming likely plays a role. On the other side, lower values of ∼5% are found in high luminosity ($L_{2500\ \text{Å}} > 10^{31}$ erg s^{-1} Hz^{-1}, Yuan et al. 1998) and high redshift ($z > 4$, Vignali et al. 2002; Steffen et al. 2006) quasars. In Fig. 12c we show the case for an X-ray-quiet source, with $f_X = 5\%$ and the other parameters as in the baseline study. The allowed region is increased, because lower X-ray emission implies a lower ionization parameter. This is important especially at low BH masses, where the requirements to avoid gas over-ionization are more stringent.

(d) Wind inner radius: We changed the inner wind radius from 100 R_S to 300 R_S (Fig. 12d). The allowed wind region is smaller than in our baseline study, because part of the parameter space is excluded both at high BH masses (as is apparent from a comparison with Fig. 11), where a wind cannot be launched because the physical distance of the gas is too large for the radiation pressure to be effective.

Summarizing, our results indicate that only a limited range of physical conditions can give rise to a radiation driven wind in AGNs, but also that these conditions do exist, and are the same as those observed in AGN warm absorbers, and needed for a warm gas that pressure confines the BEL gas. Furthermore, we showed how our simple approach can provide an immediate physical understanding of the dependence of the wind on the individual initial parameters.

The analytical results presented here have several important limitations, as noted at the start of Sect. 4. In addition, our treatment is based on a condition of existence for the solutions of the equation of motion of a wind element. This is a less stringent condition than requiring an actual wind solution for a given set of initial parameters. As a result, real wind solutions are possible only for smaller parameter regions than those shown in Figs. 11 and 12. Importantly though, no real solution outside these regions should exist. The exception is for $\epsilon_{\rm EDD} \geq 1$, for which a wind can be accelerated through electron scattering alone.

5. Comparison with previous results

A comparison of our results with those obtained with more complex hydrodynamical codes is useful to test the reliability of *QWIND*. In particular, we refer to the work of P00, in which a radiation-driven wind from a SS disk is studied, solving the wind equations through a 2-dimensional hydrodynamical code.

The properties of the solutions are remarkably similar. In particular:

- The velocity profile in P00 (their Fig. 2) is remarkably similar, after the wind has bent towards the radial direction. In particular, when the external force becomes effective, and the gas changes its direction, the velocity very rapidly increases up to its maximum value (around 10^4 km s^{-1}). This agrees with our main approximation, i.e. the separation between a internal pressure-dominated phase and an external radiation-force-dominated phase.
- The ionization parameter profiles are quite similar. This is not surprising, and indeed is only a check of self-consistency, since we have adopted the same assumptions for the X-ray cross-section as P00. As discussed above, in this scenario the ionization parameters rapidly drops from large ($>10^5$) to very low ($<10^3$) values across a thin layer of $N_{\rm H} \sim 10^{22}$ cm^{-2}.
- The final values for the ejected mass are comparable. We find for our "case study" a value of ∼1 $M_\odot$ yr^{-1}, which is close to that of P00 for the same black hole mass. (Note that the mass loss rate scales as $M_{\rm BH}^2$).

Summarizing, the comparison with the results of P00 shows that our model qualitatively agrees with a much more complex and more precise treatment. Given the huge uncertainties in the initial conditions (both regarding the structure of the disk and the mechanism of initial launching of the gas), we believe our approach is well supported. We remind the reader, however, that our simplified approach should be used as a way to quickly explore and physically understand the possible solutions, while a more detailed treatment is needed if one is interested in the precise values of the parameters involved or in more detailed structure.

6. Conclusions, and future work

We have shown that a radiation-driven wind can be accelerated to velocities of about 10^4 km s^{-1} from a Shakura-Sunyaev accretion disk at a distance from the central black hole close to that of the BEL clouds, for densities and temperatures in the range observed in quasar warm absorbers.

Thanks to our simple approach, we were able to make an analytic estimate of the parameter space in which a wind solution is allowed, and to build a fast code, *QWIND*, which can be used to better investigate the dependence on the several unknown initial parameters.

The main limitation of our study is the assumption of a substantial initial velocity (a few 100 km s^{-1}) which makes the wind supersonic from the beginning. We did not discuss the physical mechanism through which the disk provides the initial kinetic energy to the gas.

Our main results are:

1. Our model reproduces the global results of more complex hydrodynamical codes. This makes us confident that our approach can be used to explore the potentially huge space of initial conditions, in order to understand in which cases a wind can be launched. The results of our analytical study agree with those of the numerical code *QWIND*, in the sense that the parameters space regions excluded by the analytical analysis are also excluded with the more precise numerical approach.
2. For initial parameters typical of AGN warm absorbers, a wind can arise only for relatively high accretion efficiencies ($\epsilon_{\rm EDD} > 0.3$) and in a *narrow range of disk radii*. This is due to overionization at smaller radii, and to a too small a UV radiation field and initial velocity at larger radii, and is an inherent feature of radiation driven disk winds in AGNs.
3. The inner part of the gas, which is too overionized to be effectively accelerated, forms a "failed wind" which removes the X-ray radiation from directions close to the disk plane,

allowing a fast decrease of the ionization parameter with the distance form the central source, and so allowing the line driven wind acceleration at larger radii. This component fulfills the function of the "hitchhiking gas" postulated by Murray & Chiang (1995).

4. We have shown how QWIND can be used to gain a simple physical understanding of the dependence of the wind properties on the initial parameters, such as the X-ray to UV ratio, the Eddington ratio, the initial density and temperature, the central black hole mass. Some of the results are at first counter-intuitive, as, for example, the non-monotonic dependence of the wind final velocity on the Eddington ratio: in some cases more luminous sources can have slower winds, with the other physical parameters being held constant.
5. The terminal velocity of the wind is typically $1-2 \times 10^4$ km s^{-1}, and the cone covering factor is a few percent of the lines of sight. This is in reasonable agreement with observations of BAL quasars.
6. The wind angle above the disk is substantial (~20 deg), and so is neither equatorial nor polar. Some ~35% of the viewing directions will see the X-ray and UV continuum source through the wind.

Our findings could have deep implications for wind-embedded BEL models, like that of Elvis (2000). Black holes accreting in conditions outside the narrow allowed ranges would not have winds, and so neither absorption lines nor the BELs would be observed. Such "naked quasars" would be picked up from their non-stellar colors in the Sloan Digital Sky Survey or by their high X-ray flux in X-ray surveys. A few "lineless" quasars have been found but they are rare (e.g. McDowell et al. 1995). If AGN winds are radiation-driven, then some self-regulation mechanism must be involved in the accretion process, to keep the AGNs at the conditions needed for a radiation driven wind.

Our main aims at this stage were to check the reliability of our approach, and to give significant examples of its use. The next major step, which will be presented in a forthcoming paper, is a systematic survey of initial parameters, to give a more general view of the physical conditions needed to accelerate winds by line driving. In particular, we will investigate how the results are affected by changes in the wind inner radius and in the initial density and velocity profiles.

Acknowledgements. We are grateful to Jonathan Mc Dowell for his help with the numerical code, and to the anonymous referee for his/her comments and a close reading of the text, which greatly improved the clarity of the work. This work has been partially supported by NASA grants NNX08AX78G, NNX07AI22G and GO7-8136A, and by grant ASI-INAF I/088/06/0.

References

Abbott, D. C. 1982, ApJ, 259, 282
Arav, N., de Kool, M., Korista, K. T., et al. 2001, ApJ, 561, 118
Antonucci, R. 1993, ARA&A, 31, 473
Baldwin, J. A. 1977, ApJ, 214, 679
Bechtold, J., Siemiginowska, A., Shields, J., et al. 2003, ApJ, 588, 119
Blandford, R. D., & Payne, D. G. 1982, MNRAS, 199, 883
Brotherton, M. S. 1996, ApJS, 102, 1
Castor, J. I., Abbott, D. C., & Klein, R. I. 1975, ApJ, 195, 157
Crenshaw, D. M., Kraemer, S. B., Boggess, A., et al. 1999, ApJ, 516, 750
Dorodnitsyn, A., Kallman, T., & Proga, D. 2008, ApJ, 687, 97
Elvis, M., et al. 1994, ApJS, 94, 1
Elvis, M. 2000, ApJ, 545, 63
Everett, J. E., & Murray, N. 2007, ApJ, 656, 93
Fukue, J., & Akizuki, C. 2006, PASJ, 58, 1039
George, I. M., Turner, T. J., Mushotzky, R. et al. 1998, ApJS, 114, 73
Hamann, F., Korista, K. T., & Morris, S. L. 1993, ApJ, 415, 541
Hawley, J. F., & Krolik, J. H. 2006, ApJ, 641, 103
Icke, V. 1980, AJ, 85, 329
Konigl, A., & Kartje, J. F. 1994, ApJ, 434, 446
Krongold, Y., Nicastro, F., Brickhouse, N. S., et al. 2003, ApJ, 597, 832
Kurosawa, R., & Proga, D. 2009, MNRAS, 397, 1791
Laor, A., Fiore, F., Elvis, M., Wilkes, B. J., & McDowell, J. C. 1997, ApJ, 477, L93
Lee, L. W., & Turnshek, D. A. 1995, ApJ, 453, L61
Maloney, P. R., Hollenbach, D. J., & Tielens, A. G. G. M. 1996, ApJ, 432, 606
Mathur, S., Elvis, M., & Wilkes, B. 1995, ApJ, 452, 230
Maiolino, R., Salvati, M., Marconi, A., et al. 2001, A&A, 375, 25
McDowell, J. C., Canizares, C., Elvis, M., et al. 1995, ApJ, 450, 585
Mineshige, S., & Shields, G. A. 1990, ApJ, 351, 47
Murray, N., & Chiang, J. 1997, ApJ, 474, 91
Nicastro, F., Fiore, F., Perola, G. C., et al. 1999, ApJ, 512, 184
Netzer, H., Chelouche, D., George, I. M. 2002, ApJ, 571, 256
Ogle, P. M., Cohen, M. H., Miller, J. S., et al. 1999, ApJS, 125, 1
Ohsuga, K., Mori, M., Nakamoto, T., et al. 2005, ApJ, 628, 368
Ohsuga, K., Mineshige, S., Mori, M., & Kato, Y. 2009, PASJ, 61, L7
Osmer, P. S., & Shields, J. C. 1999, in Quasars and Cosmology (San Francisco: ASP), ASP Conf. Ser. 162, 235
Panessa, F., & Bassani, L. 2002, A&A, 394, 435
Pounds, K. A., Reeves, J. N., King, A. R., et al. 2003, MNRAS, 345, 705
Proga, D. 2003, ApJ, 585, 406
Proga, D., & Kallman, T. R. 2004, ApJ, 616, 688
Proga, D., Stone, J. M., & Drew, J. E. 1998, MNRAS, 295, 595
Proga, D., Stone, J. M., & Kallman, T. R. 2000, ApJ, 543, 686
Reynolds, C. S. 1997, MNRAS, 286, 513
Risaliti, G., Elvis, M., & Nicastro, F. 2002, ApJ, 571, 234
Risaliti, G., & Elvis, M. 2004, Supermassive Black Holes in the Distant Universe, 308, 187
Rokaki, E., Lawrence, A., Economou, F., et al. 2003, MNRAS, 340, 1298
Rudge, C. M., & Raine, D. J. 1998, MNRAS, 297, L1
Shakura, N. I., & Sunyaev, R. A. 1973, A&A, 24, 337
Schurch, N. J., & Done, C. 2007, MNRAS, 381, 1413
Siemiginowska, A., Czerny, B., & Kostyunin, V. 1996, ApJ, 458, 491
Smith, P. S., Schmidt, G. D., Hines, D. C., et al. 2003, ApJ, 593, 676
Stone, J., & Norman, M. 1992, ApJS, 80, 753
Stevens, I. R., & Kallman, T. R. 1990, ApJ, 436, 599
Tajima, Y., & Fukue, J. 1996, PASJ, 48, 529
Vignali, C., Brandt, W. N., Schneider, D. P., Garmire, G. P., & Kaspi, S. 2003, AJ, 125, 418
Wandel, A. 2002, ApJ, 565, 762
Wandel, A., Peterson, B. M., & Malkan, M. A. 1999, ApJ, 526, 579
Watarai, K.-Y., & Fukue, J. 1999, PASJ, 51, 725
Weymann, R. 1997, Mass Ejection from Active Galactic Nuclei, ASP Conf. Ser., 128, 3
Wills, B. J., & Browne, I. W. A. 1986, ApJ, 302, 56
Young, M., Elvis, M., & Risaliti, G. 2010, ApJ, 708, 1388
Yuan, W., Brinkmann, W., Siebert, J., et al. 1998, A&A, 330, 108
Zamorani, G., Henry, J. P., Maccacaro, T., et al. 1981, ApJ, 245, 357